Soft Matter

PAPER

View Article Online
View Journal | View Issue

Cite this: *Soft Matter*, 2025, **21**, 6613

Thermodynamic investigation of renewable block copolymers based on poly(lactic acid) and poly(ethylene azelate)†

Rafail O. Ioannidis,[a] Panagiotis A. Klonos,*[ab] Zoi Terzopoulou,[ac] Nikolaos Nikolaidis,[a] Apostolos Kyritsis[b] and Dimitrios D. Bikiaris*[a]

We studied a recently synthesized series of diblock copolymers based on poly(ethylene azelate) (PEAz) and poly(lactic acid) (PLA), prepared *via in situ* ring-opening polymerization of L-lactide in the presence of low-molecular-weight PEAz (5 kg mol^{-1}). The initial PEAz amount varied from 2.5 up to 20%. The materials are envisaged for use in biomedical applications, so we aimed to manipulate the overall properties (glass transition, crystallizability) and improve the compostability of PLA, with the latter being required for green chemistry and the circular economy. A series of structural and thermodynamic techniques were employed. Regarding novelty, molecular dynamics mapping for PEAz-*b*-PLA and neat PEAz is presented here for the first time. The PEAz-*b*-PLA copolymers were generally found to be quite homogeneous systems with respect to their thermal transitions. The crystal nucleation and fraction are suppressed in the copolymers, most probably due to the reduction in M_n, while alterations in the semicrystalline morphology were recorded. As for the amorphous polymer mobility, the glass transition temperature (calorimetric and dielectric, from ~60 to ~25 °C) and the fragility index of PLA (hard component) both fall systematically in the presence of PEAz. It is estimated that the *in situ* copolymerization, the presence of PEAz (soft component), and the simultaneous reduction in the average molecular weight (12–76 kg mol^{-1}) lead to an increase in the free volume in the copolyesters. The overall results provide firm indications of the plasticizing role of PEAz on PLA, which is one of the general goals for such copolymers. Overall, using these copolyesters, there is an opportunity for targeted structural manipulation (thermochemically mild) connected to the material's macroscopic performance.

Received 24th June 2025,
Accepted 7th July 2025

DOI: 10.1039/d5sm00646e

rsc.li/soft-matter-journal

1. Introduction

Polymers and polymer-based materials have been essential to humanity for over a century, fulfilling numerous needs in industry, academia, and everyday life.[1–3] However, traditional polymers, widely known as 'plastic', are mainly produced from non-renewable resources (*i.e.*, fossil-based petrochemicals).[4] This fact, combined with the extensive use of plastics by the growing population, in terms of both numbers and needs, has resulted in a severe environmental threat. The threat arises from the extensive accumulation of plastic waste in nature, mainly in the sea and the soil.[5,6] Over the past two decades, increasing global environmental awareness has focused attention on developing, studying and applying polymers prepared from renewable resources,[7,8] with an emphasis on non-toxicity and recyclability. This relatively new family of polymers is called 'green polymers'[9–11] and is meant to serve the modern global economic strategy, *i.e.*, the 'green economy'.[12,13]

Among the most well-known green polymers are polyesters, such as poly(lactic acid) (PLA),[14–16] poly(ε-caprolactone)[17,18] and, more recently, polyesters prepared from succinic acid, adipic acid, furan-dicarboxylic acid, vanillic acid[6,19–22] and azelaic acid.[23] PLA, the polymer of interest herein, has proved its high value as it has been implemented across a wide range of applications.[24–30] As well as being derived from renewable resources, for example, starch, sugar cane, and beet,[31,32] and produced in large scale *via* relatively mild methods, *e.g.*, ring-opening polymerization (ROP),[33] PLA exhibits good thermal/chemical stability[34] and mechanical performance,[35] with

[a] Department of Chemistry, Laboratory of Polymer Chemistry and Technology, Aristotle University of Thessaloniki, GR-541 24, Thessaloniki, Greece. E-mail: pklonos@central.ntua.gr, dbic@chem.auth.gr
[b] Department of Physics, National Technical University of Athens, Zografou Campus, GR-15780, Athens, Greece
[c] Laboratory of Industrial Chemistry, Department of Chemistry, University of Ioannina, GR-45110, Ioannina, Greece

† Electronic supplementary information (ESI) available. See DOI: https://doi.org/10.1039/d5sm00646e

moderately low glass transition (T_g) and melting (T_m) points.[36–39] The performance of PLA is closely linked to its semicrystalline character, with the latter having been found to be quite easily tunable. This tuning can be achieved by altering its molecular weight[30,38,40–42] and, more easily, by proper thermal treatment. The degree of crystallinity, the semicrystalline morphology, and the degree of crystal interconnectivity are the key factors affecting macroscopic performance, including mechanical performance, permeation of small molecules, and thermal conductivity.[43–45]

As expected, PLA also has disadvantages, particularly its lack of fast physical degradation in soil/sea conditions, mainly owing to its rigid structure (glassy with small free volume fraction), hydrophobicity and semi-crystallinity. These factors preclude the fast hydrolytic/enzymatic scission of the ester bonds[38,46] and, thus, its depolymerization. This problem can be overcome, and a proven strategy involves combining PLA with other renewable polymers (mainly polyesters) in the form of polymeric blends and copolymers.[47–53] The addition of a lower-T_g component combined with a proper mixing or copolymerization method (*e.g.*, *in situ* polymerization) has been proven to be quite efficient in the manipulation of the overall performance.

In this direction lays the present basic research work, which belongs in the general framework of our groups. In particular, here we investigate a series of diblock copolyesters that we recently prepared[54,55] based on PLA and poly(ethylene azelate), PEAz, by initiating with PEAz of low molar mass and performing *in situ* ROP of L-lactide (PEAz-*b*-PLA). The PLA/PEAz ratio of the samples ranges from 97.5/2.5 to 80/20. Simultaneously, we also studied PEAz and PLA. For this study, we employed the following characterization techniques: differential scanning calorimetry (standard DSC and temperature-modulated DSC (TMDSC)), X-ray diffraction (XRD), polarized light microscopy (PLM), Fourier transform infra-red spectroscopy (FTIR), and broadband dielectric spectroscopy (BDS). The molecular dynamics mapping for PEAz and the copolymers is performed here for the first time.

2. Experimental

2.1. Materials and synthesis

2.1.1. Materials. Azelaic acid (AzA) (purity: >99.0%) was supplied by Fluka (Steinheim, Germany). 1,2-Ethanediol (anhydrous, >99.8%), 1-dodecanol and tin(II) 2-ethylhexanoate ($Sn(Oct)_2$) were purchased from Aldrich Co., (London, UK). Titanium butoxide ($Ti(OBu)_4$, purity: >97.0%) was purchased from Sigma Aldrich Chemical Co (Steinheim, Germany), and L-lactide (LA) (99.9%) was purchased from PURAC Biochem BV (Gorinchem, The Netherlands) under the brand name PURASORBsL. All other materials and solvents used were of analytical grade.

2.1.2. Synthesis of PLA, PEAz and copolyesters. PEAz and PLA were synthesized employing a two-stage melt polycondensation procedure (esterification and polycondensation), and ring-opening polymerization (ROP) of L-lactide. For the synthesis of PEAz, azelaic acid and 1,2-ethanediol were used in a weight ratio of 1/1.1 in the presence of 400 ppm TBT, while in the case of PLA, L-lactide, 400 ppm of $Sn(Oct)_2$ and 0.05 g of 1-dodecanol were added to the polymerization apparatus. A series of two-block copolymers, PLA-*b*-PEAz copolyesters, was synthesized *via* the *in situ* ROP of L-lactide using the synthesized PEAz of low molecular weight, $M_n \sim 5$ kg mol^{-1}, as the macroinitiator and 400 ppm of $Sn(Oct)_2$ as the catalyst, at four different PLA/PEAz weight ratios, *i.e.*, 97.5/2.5, 95/5, 90/10 and 80/20 w/w. The synthetic process is described in detail in a recently published work.[54] For the copolymers, the ROP conditions are kept identical (temperatures, time periods), thus, when gradually increasing the initial amount of PEAz, the development of PLA blocks initiates from gradually increasing number of points (side groups of PEAz) and, consequently, the length of the final PLA blocks gradually decreases. This is reflected in the measured lowering of M_n (from ~80 down to 12 kg mol^{-1}, Fig. 1) and the reduction of the corresponding intrinsic viscosities, [η] (from 1.89 to 0.82 dL g^{-1}).[54] For comparison, we prepared neat PLA under the same ROP conditions (Fig. 1).

The samples were received in the form of films, and were additionally formed as cylindrical pellets of ~25 mm in

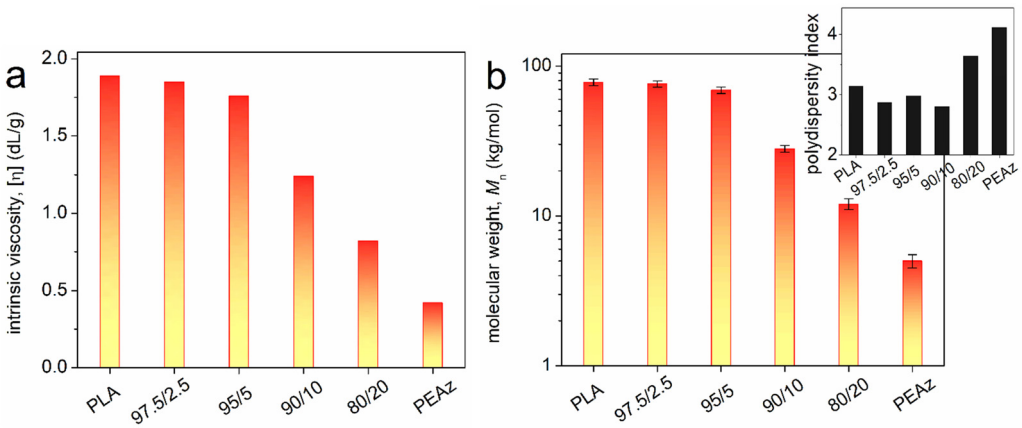

Fig. 1 (a) Intrinsic viscosity, [η] and (b) number average molecular weight, M_n, for the systems studied herein. The inset to (b) shows the corresponding data for the polydispersity index (PDI), $Đ$. Data adapted and reproduced from ref. 54 with permission from the Royal Society of Chemistry.

diameter and ~1.5 mm in height (thickness), prepared using a special mold, upon melting (employing a thermal press) and rapid cooling in cold water.

2.2. Experimental techniques

The complementary techniques and analysis methods employed in this work are described in detail in Section S1 of the ESI,† whereas, below, the techniques are reported in brief.

The ATR-FTIR spectra in the wavenumber range from 4000 to 500 cm^{-1} and at a resolution of 2 cm^{-1} were recorded for melt-quenched samples by means of a IRTracer-100 spectrophotometer from Shimadzu (Kyoto, Japan) equipped with a QATR™ 10 Single-Reflection ATR accessory with a diamond crystal.

Conventional and temperature-modulated differential scanning calorimetry (DSC and TMDSC) were employed to study the thermal transitions, namely, glass transition, crystallization, and melting, within the temperature range from −190 to 190 °C. Two thermal protocols were used for DSC and one for TMDSC: scan 1, involving a fast cooling and heating at 10 K min^{-1}; scan 2, with standard linear cooling at 10 K min^{-1} and heating at 10 K min^{-1}; scan 3, using TMDSC, involved heating the initially melt-quenched samples at 2 K min^{-1} with a temperature modulation period of 1 min and amplitude of 1 K. The measurements were performed by means of a TA Q200 calorimeter (TA Instruments, USA).

XRD was employed to study the crystalline structure and estimate the degree of crystallinity. The measurements were performed on melt-crystallized samples (as in DSC scan 1) using a MiniFlex II XRD system (Rigaku Co, Tokyo, Japan) in the 2θ angle range from 5° to 45°.

The PLM method was employed to evaluate any changes in the semicrystalline morphology for both melt- and cold-crystallized samples. The corresponding micro-images were captured using a Nikon Optiphot-1 polarizing microscope equipped with a Linkam THMS 600 heated stage, a Linkam TP91 control unit and a Jenoptic ProgRes C10Plus camera.

BDS[56] was employed to assess the molecular dynamics of PLA and PEAz in bulk and within the copolymers, employing a Novocontrol BDS setup (Novocontrol GmbH, Germany). The measurements were conducted on melt-quenched systems at various temperatures ranging from −150 to 120 °C upon heating and over a broad frequency range from 10^{-1} to 10^{6} Hz.

3. Results and discussion

3.1. Materials and structure

Recent work by our groups showed that a quite effective route to prepare copolymers (di- and tri-blocks) with minor or absent phase separation is the *in situ* polymerization of one of the polymers in the presence of an existing polymer of relatively low molecular weight, M_n. In our case, the initial block consists of PEAz with M_n ~ 5 kg mol^{-1} (Scheme 1). The *in situ* ROP of lactide indeed led to the formation of PEAz-*b*-PLA copolymers. By keeping the thermochemical conditions of the ROP fixed and by increasing the amount of PEAz it is essential that we

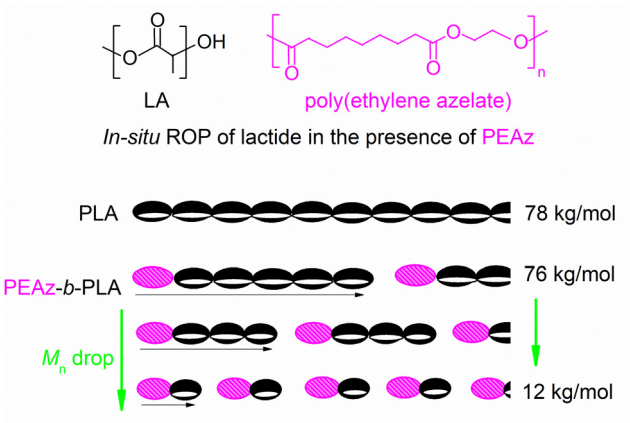

Scheme 1 Schematic view of the PEAz-*b*-PLA copolymers under investigation, displaying the highest and lowest molecular weight values.

create gradually more PEAz-*b*-PLA entities of, however, shorted PLA blocks (Scheme 1), or else, of overall smaller M_n. Compared to neat PLA prepared under the same conditions, which exhibits a relatively high M_n of 78 kg mol^{-1}, the measured M_n in the copolymers drops monotonically to 12 kg mol^{-1} (Fig. 1).[54] At the same time, the intrinsic viscosity of PLA (hard polymer, higher T_g component) drops, both due to the addition of the softer polymer and the simultaneous drop of M_n (Fig. 1).[54] Considering the drop in intrinsic viscosity of PLA as well as other structural facts, we believe that the copolymer synthesis was successful. It is expected that the thermodynamic study will provide more evidence of the successful synthesis.

We performed ATR-FTIR measurements on the initially amorphous samples. The results are presented in Fig. 2(a). In the copolymers, the FTIR absorption response is dominated by the presence of PLA, as expected due to the high amount of PLA (80–97.5 wt%). In particular, we observed the responses arising from the –CH, –C=O and C–O bond vibrations at around 3000, 1750 and 1000 cm^{-1}, respectively (Fig. 2(a)). The overall results are in accordance with previous findings on PLAs[53,57,58] (and references therein).

In polyesters, the most polar site is usually the ester. The ester bond (–C=O) vibration, particularly any alterations in its wavenumber position and the width of the wavenumber band recorded in homopolymers and other complex systems,[59–61] provides valuable information for the implementation of the ester site within interactions (chain–chain, interfacial, crystal nucleation-related, *etc.*).

In our case, in Fig. 2(b), upon the proper normalization, first, the corresponding peak of neat PEAz (~1726 cm^{-1}) is not individually recorded in any of the copolymers. The peak for PLA (~1747 cm^{-1}) is the dominant one for PLA and the copolymers. We did not record any significant migration toward lower wavenumbers (toward more bound bonds). However, there seems to be a small contribution of absorbance on the main peak in that direction. The effect is worth noting in the case of the 80/20 copolymer. We can conclude that there is some homogenization of the vibrational character of the ester bond and a very weak tendency for inter-chain interactions.

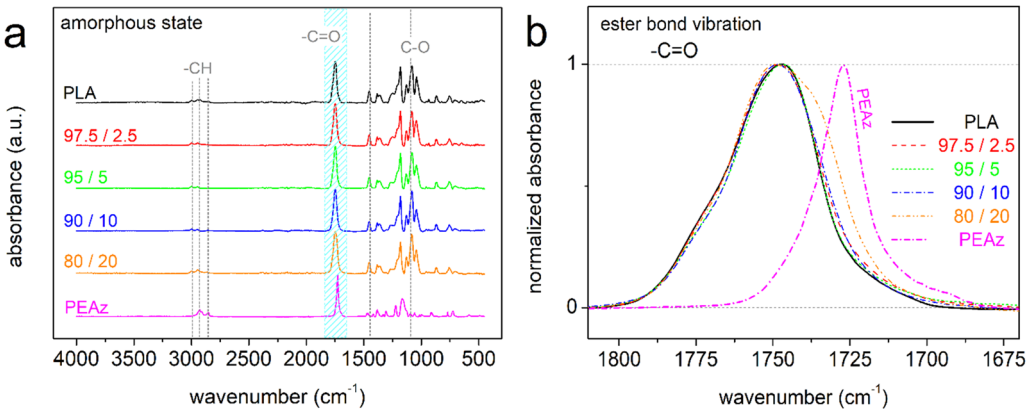

Fig. 2 (a) ATR-FTIR spectra for PLA, PEAz and PLA-*b*-PEAz in the initially amorphous state. The origins of the stronger absorbance bands are marked. (b) Zoomed region focusing on the ester bond (–C═O) absorbance band.

3.2. Glass transition and crystallization

The calorimetric results are presented in Fig. 3. For comparison to the thermal events of the PLA/PEAz copolymers, we included the results for neat PLA and neat PEAz. As both polymers are semicrystalline, we chose to perform two sets of measurements, *i.e.*, one involving fast cooling aiming at the suppression of crystallization (non-linear 80–100 K min^{-1}, scan 1) and another one involving standard linear cooling (10 K min^{-1}, scan 2). If achieved, the elimination of crystallization enables the evaluation of the effects of the direct polymer structure (composition, M_n, *etc.*) on the glass transition. In neat PLA, the fast cooling (Fig. 4(a)) was successful in eliminating crystallization and the same was also true in the PLA-rich copolymers. By contrast, PEAz exhibits a stronger crystallinity character with the

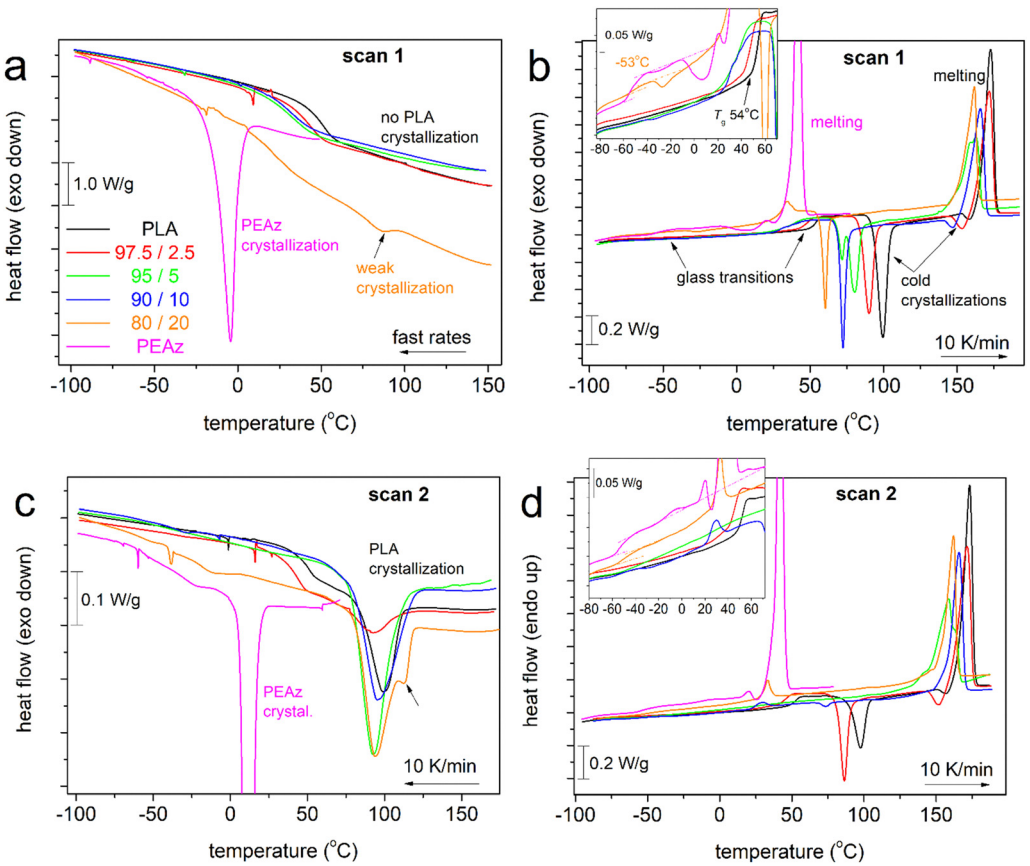

Fig. 3 Overall DSC results in terms of comparative cooling/heating curves for all samples. The data are grouped and shown for (a), (b) scan 1 and (c), (b) scan 2. The insets to (b), (d) show the regions of the glass transitions in better resolution. The heat flow is presented upon normalization to the mass of the sample.

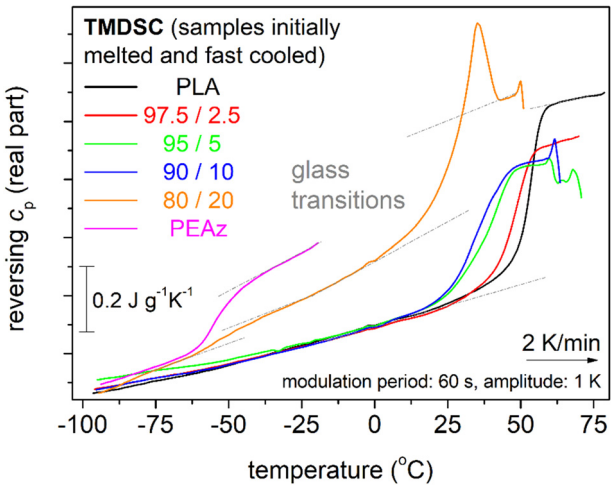

Fig. 4 TMDSC results in terms of the temperature evolution of the reversing part of heat capacity, $c_{p,rev}$, for all samples and the described modulation parameters.

corresponding crystallization peak (T_c) being recorded at −4 °C (scan 1) or 12 °C (scan 2). Comparing the corresponding enthalpy changes during crystallization, ΔH_c (eqn (S1) and tables in Section S2 in the ESI†), with the bibliographic value for the heat of fusion for 100% crystalline PEAz, $\Delta H_{100\%}$ = 160 J g^{-1},[62] the crystalline fraction, CF_c, of PEAz equals 37% (scan 1) or 43% (scan 2). For neat PLA, the melt crystallization is recorded only upon slower cooling, more precisely, at T_c = 99 °C with CF_c = 21%.

For the copolymers, it can be clearly seen in Fig. 3 that PLA exhibits crystallization peaks and glass transition steps in all cases, whereas PEAz exhibits crystallization only in the 80/20 w/w sample (Fig. 3(c)) and a glass transition (insets in Fig. 3(b) and (d)) in the 80/20 w/w and 90/10 w/w samples. This suggests that there could be partial phase separation in the latter samples, in particular, micrometric in 80/20 and at least nanometric in 90/10. It is important to report that such phase separation has been recorded before in PLA-based di- and triblock copolymers[63,64] and was found to be 'crystallization-driven', namely, to exist in the semicrystalline state, but not in the amorphous state.

The various effects have been evaluated in terms of crystallization temperatures and fractions, glass transition temperatures, T_g, and heat capacity changes, Δc_p. For the glass transition, recorded between complex phenomena using conventional DSC, we additionally performed TMDSC measurements on melted and fast-cooled samples. This type of measurement enables sufficient disentanglement of the reversing (glass transition) and non-reversing (peaks) contributions to heat capacity.[65] In Fig. 4, we present a plot of the 'reversing

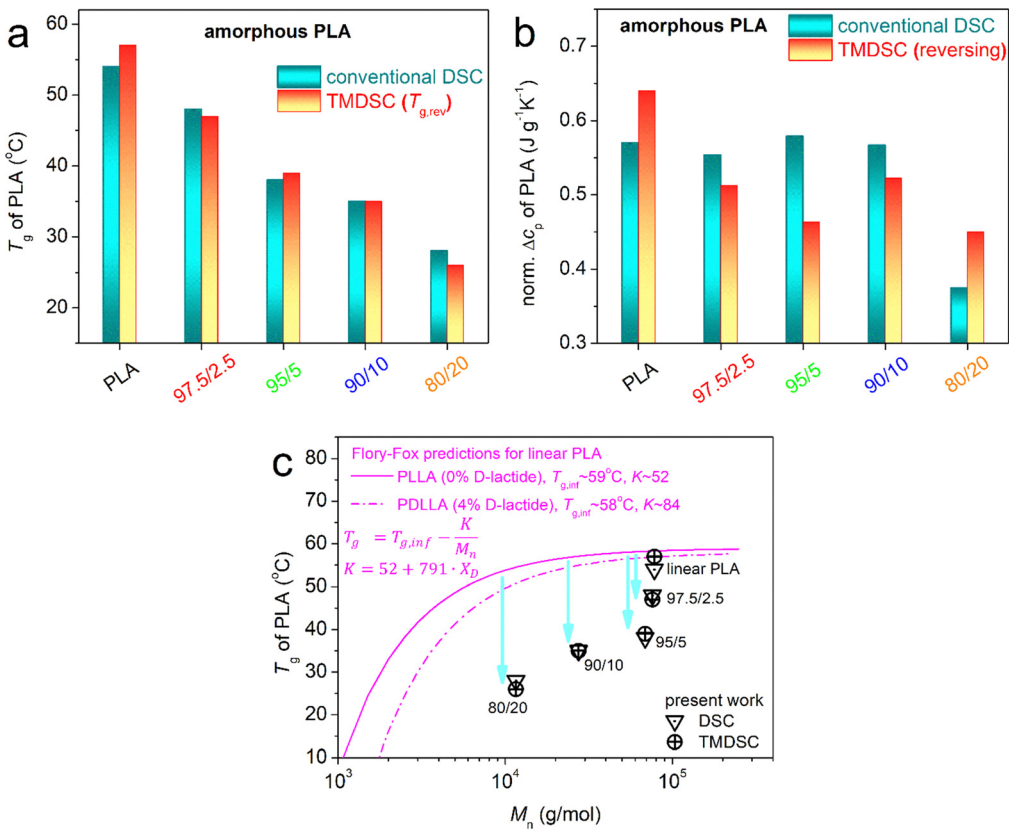

Fig. 5 (a) and (b) Selected DSC/TMDSC values related to the glass transition of PLA, namely, (a) T_g and (b) Δc_p, shown in the form of column diagrams for all samples (description on the horizontal scale axes). In (c), we compare the T_g results for different M_n (symbols) from the present work with the corresponding Flory–Fox predictions (lines).[37,64]

c_p' (also called the real part of c_p) against temperature for all samples during heating. The glass transition steps are more clearly distinguished therein. The glass transition temperature was estimated from the half c_p increase during heating.

In short, we directly discuss the effects of PEAz on the various values (Fig. 5 and 6). For the glass transition in the initially amorphous state, the calorimetric T_g of PLA (52–54 °C) in the PLA/PEAz steadily decreases with increasing PEAz (Fig. 5(a)) down to 26–28 °C. Simultaneously, the calorimetric strength of the glass transition, Δc_p, shows a tendency to decrease from ~0.6 down to ~0.45 J g^{-1} K^{-1} (Fig. 5(b)).

While the T_g drop seems compatible with the M_n reduction in the copolymers, due to easier mobility of less entangled chains, the Δc_p drop is not.[42,66] Therefore, the results indicate that more parameters in addition to M_n affect the molecular mobility. In Fig. 5(c), we compare the T_g (M_n) dependence of our systems with those of neat linear PLAs in the amorphous state prepared by the same ROP route[42] as well as other methods.[37] The results for our neat PLA follow the expected trend (lines in Fig. 5(c)). The results for the PLA-*b*-PEAz, however, exhibit lower T_gs. Moreover, the difference from neat linear homo-PLAs is systematically larger when increasing the amount of PEAz. Most probably, this reflects an additional stronger and direct effect of PEAz.

An overall interpretation of the mobility effects will be provided in the following sections based on the light shed by the segmental dynamics (BDS) results.

Next, we examine the effects on crystallization, and these can be discussed with reference to the composition trends shown in Fig. 6. The melt crystallization temperature in Fig. 6(a) exhibits a general small suppression in the copolymers (92–95 °C), as compared to neat PLA (99 °C), suggesting weaker nucleation. Then, cold crystallization is strongly accelerated, as evidenced by the ~10–40 K lower T_c. The result is clearly connected to the lowering of T_g, which can be explained as follows: cold crystallization results from a prior significant supercooling during cooling, which leads to the formation of large numbers of crystal nuclei, and enables crystal growth as soon as the amorphous chains become mobile (during the transition from the glassy to rubbery/liquid state). The latter occurs earlier (at lower T) as the PEAz increases in the copolymers. The overall effects are expected considering, at least, the M_n reduction in the copolymers.

The 'crystalline fraction of PLA' was calculated and is shown in Fig. 6(b), assuming that the corresponding exo- and endothermal peaks recorded at $T > T_g$ in the copolymers, correspond to the cold crystallization and melting, respectively (eqn (S1) in the ESI†). The results show that CF during cold crystallization of scan 1 decreases in the copolymers, whereas the CF during melt crystallization (scan 2) mainly increases, and is almost doubled in the 95/5, 90/10 and 80/20 w/w samples. The situation for the total CF of scan 2 is qualitatively similar, *i.e.*, when considering the melt and subsequent cold crystallization together. In Fig. 6(c), continuing with the above

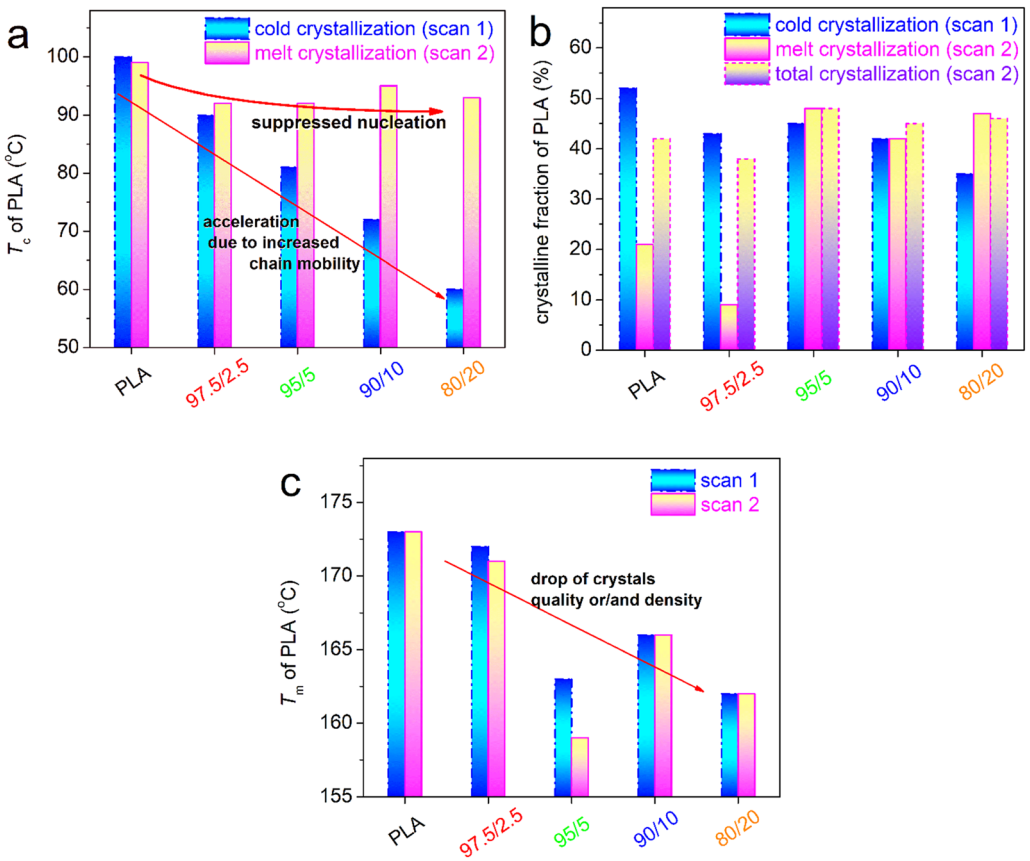

Fig. 6 DSC values related to the crystallization of PLA in the form of column diagrams, *i.e.*, (a) T_c. (b) CF and (c) T_m, for the thermal events described.

assumption, we show the effects on the melting temperature, T_m. Therein, the T_m of neat PLA (173 °C) consistently decreases when the PEAz fraction increases (159–172 °C). There is an exception to this trend in the case of 95/5 w/w. In general, the effects suggest a drop in the quality (size or/and density) of the spherulites in the copolymers. To gain clearer insights into crystallization, we employed XRD and PLM.

In Fig. 7(a) and (b), we present the XRD data for all PLA-based samples, upon being subjected to melt- (Fig. 7(a)) and cold- (Fig. 7(b)) crystallization almost identically to DSC scans 2 and 1, respectively. It is interesting to mention, from the methodological point of view, that PLA is a polymer that offers such possibilities in general.[67–69] A series of crystalline diffraction peaks were recorded for all samples, and the results are in accordance with previous results for PLA. The number of crystallization peaks in the copolymers, as compared to PLA, is mainly unchanged. Quite mild effects on the 2θ positions were also recorded, in particular, demonstrating weak migrations toward higher 2θ for the higher PEAz amount (arrows in Fig. 7(a)) and when cold crystallization is implemented (arrows in Fig. 7(b)). In these cases, we expect broadly similar crystallization mechanisms but possibly smaller 'unit cells' for the crystals. This is consistent with the DSC results shown in Fig. 3(b) and (d), which indicate that the melting temperature decreases in the copolymers and further in the cold-crystallized samples.

Additionally to these qualitative observations, XRD allowed a safer evaluation of the overall crystalline fraction, CF_{XRD}.[70] Adopting previous methodologies,[44,60,70] we analyzed the XRD spectra by proper fitting of mathematical model functions (here Lorentzians). An example of this fitting is shown in Fig. 7(c). CF_{XRD} is calculated by comparing the total areas of the crystalline diffraction peaks with the total diffraction area (crystalline and amorphous together) (eqn (S2) in the ESI†). First, the CF_{XRD} in Fig. 7(d) is smaller for melt crystallization and larger for cold crystallization. Among all systems, PLA exhibits the largest CF_{XRD}, which drops by ~10% in 97.5/2.5 w/w and remains mainly low or shows a mild increase for the rest of the copolymers. Thus, the hindered nucleation recorded by DSC in the copolymers is surely accompanied by hindered crystal formation, either in terms of the size and/or density of the crystals.

Based on these findings, we should expect minor but detectable changes in the semicrystalline morphology from PLA to the copolymers. Therefore, to complete and visualize the crystallization situation, we present the corresponding PLM results in Fig. 8 and 9, respectively, for melt- and cold-crystallized systems. In Fig. 8, we can observe the larger

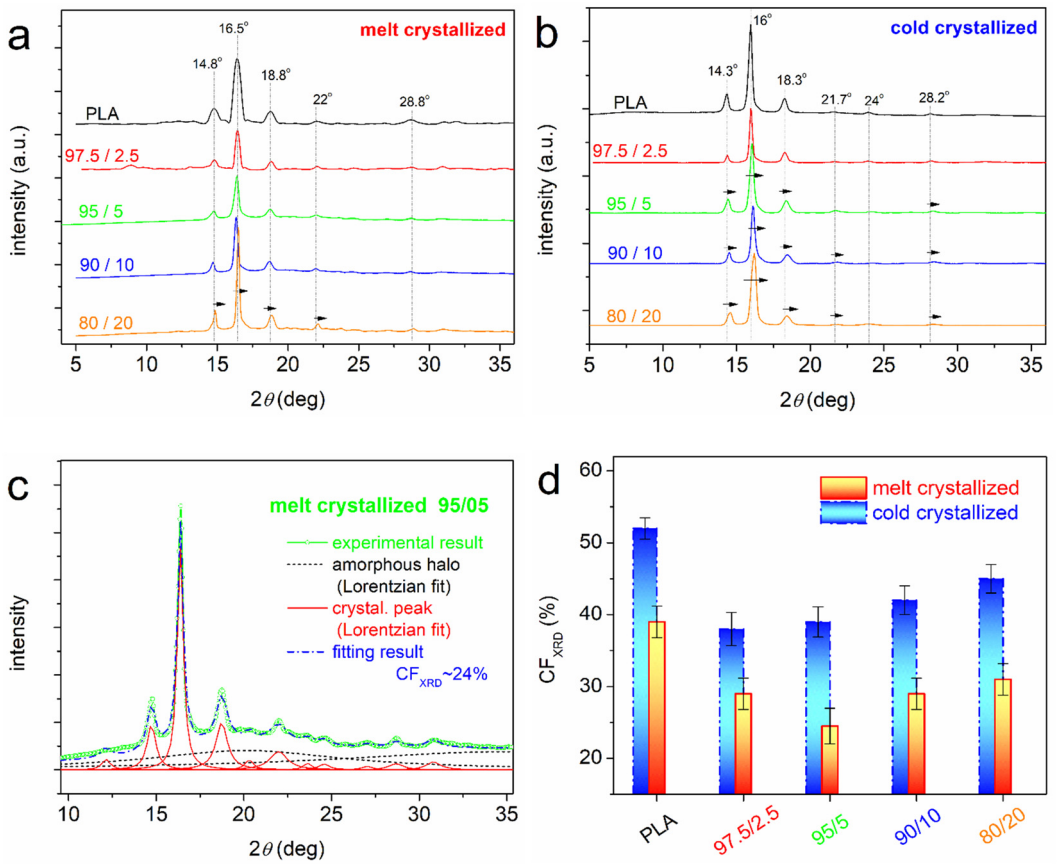

Fig. 7 Comparative XRD spectra for the PLA-*b*-PEAz copolymers and neat PLA upon being subjected to (a) melt- and (b) cold-crystallization. In (c), we present an example of the analysis of an XRD spectrum in terms of fitting by Lorentzian terms. (d) Column diagrams of the crystalline fraction as estimated by XRD.

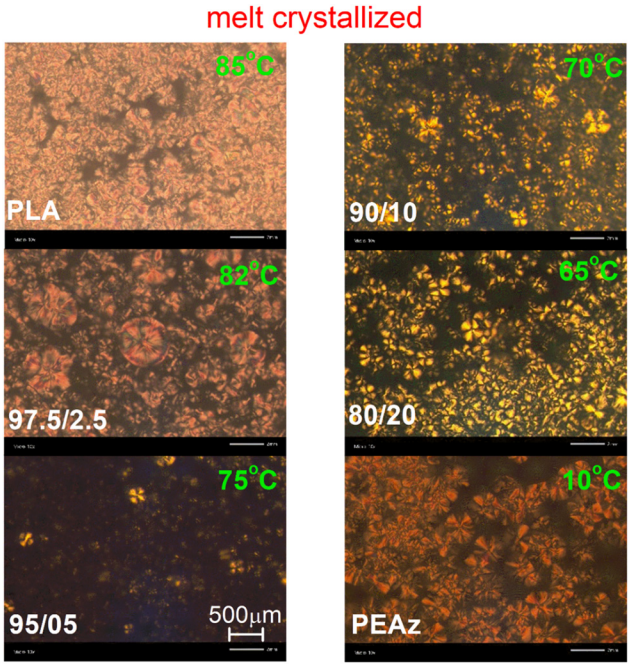

Fig. 8 PLM images for all samples subjected to melt crystallization. The images shown correspond to the final semicrystalline morphology view at the indicated temperatures.

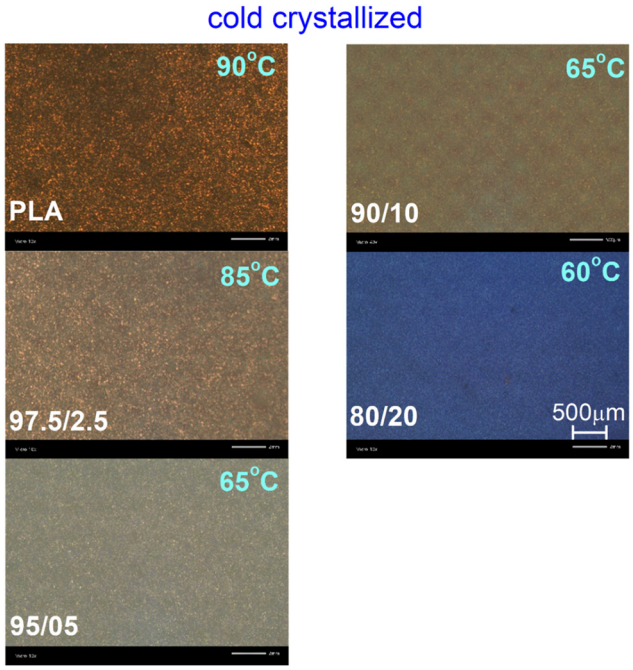

Fig. 9 PLM images for neat PLA and the PLA-*b*-PEAz copolymers subjected to cold crystallization. The images correspond to the final semicrystalline morphology view at the marked temperatures.

number of crystallites and the denser crystalline morphology in neat PLA, as compared to the copolymers. It is also visually distinguishable that the interconnectivity between the crystals is severely reduced. The latter information can be useful, as this is connected with many macroscopic properties, such as mechanical strength and thermal conduction[43,44] (and references therein).

The situation is similar for all of the cold-crystallized systems (Fig. 9), without allowing the extraction of more direct effects of the copolymer composition. The overall sample volume is filled with tiny crystals, confirming the findings from calorimetry. In particular, during cold crystallization a quite large number of crystal nuclei is activated as the polymer chains are gradually and slowly mobilized (heating). This minimizes the antagonistic effects between the crystal growing around neighbouring nuclei.[30]

3.3. Molecular dynamics

Next, we turn our attention to the BDS results. Representative results are shown in Fig. 10, in the form of $\varepsilon''(f)$ at the various T (isothermal curves, raw data). ε'' is considered to monitor the dielectric loss,[56] whereas in polymers the various dipolar-arising motions, originating from actual molecular motions, are recorded as peaks. The maxima of the peaks migrate toward higher frequencies when T increases, due to enhanced thermal/kinetic energy. Actually, the frequency distributions related to the ε'' peak correspond to the relaxation time (τ_{rel}) distributions of the followed group of dipoles.[56] For this reason, BDS is considered to indirectly monitor the 'molecular dynamics'.

Notably, the molecular dynamics of PLA have been vastly studied both in the bulk[42,71–74] as well as complex forms and under stress.[30,75–77] Contrary to that, to the best of our knowledge, the molecular dynamics of PEAz have not been mapped yet.

It is evident that the dielectric signal is low at $T < T_g$, and the dipolar response is governed by relaxations related to localized motions. In PLA, this is exemplified by the β_{PLA} process, which involves the crankshaft motion of the ester group (–C═O) on the polymer backbone.[71,72] When T approaches and exceeds T_g, there is a significant signal uprise (1–2 orders of magnitude), and the main dipolar relaxation dominates the signal. Obviously, this main relaxation is related to the mobilization of the polymer chains; it is a segmental relaxation process and, thus, is called 'α relaxation'.[56,71] The α process has been proposed to arise from the relaxation of dipole moments perpendicular to the polymer chain axis.[56,78] At even higher temperatures ($T \gg T_g$), where the viscosity of the polymer (elastic or liquid phase) is significantly decreased, additional strong phenomena related to transport of charged particles dominate. These include ionic conductivity, relaxation of interracially trapped ions, electrode polarizations, and similar effects.[56,79]

This dielectric view can be better followed and, simultaneously, compared with the calorimetric view in Fig. 11. Therein, for two selected frequencies (~0.2 and ~3.2 Hz) we have replotted ε'' as a function of T, and we can clearly distinguish the local (β_i and γ_i peaks, where i: PLA or PEAz) and segmental dynamics (α_i). By only glancing at Fig. 11, we can conclude that the α_i relaxations accelerate with the addition of PEAz (red arrows).

From the raw BDS data we can observe that in some cases the $\varepsilon''(f)$ spectra are quite complex, consisting of more than one

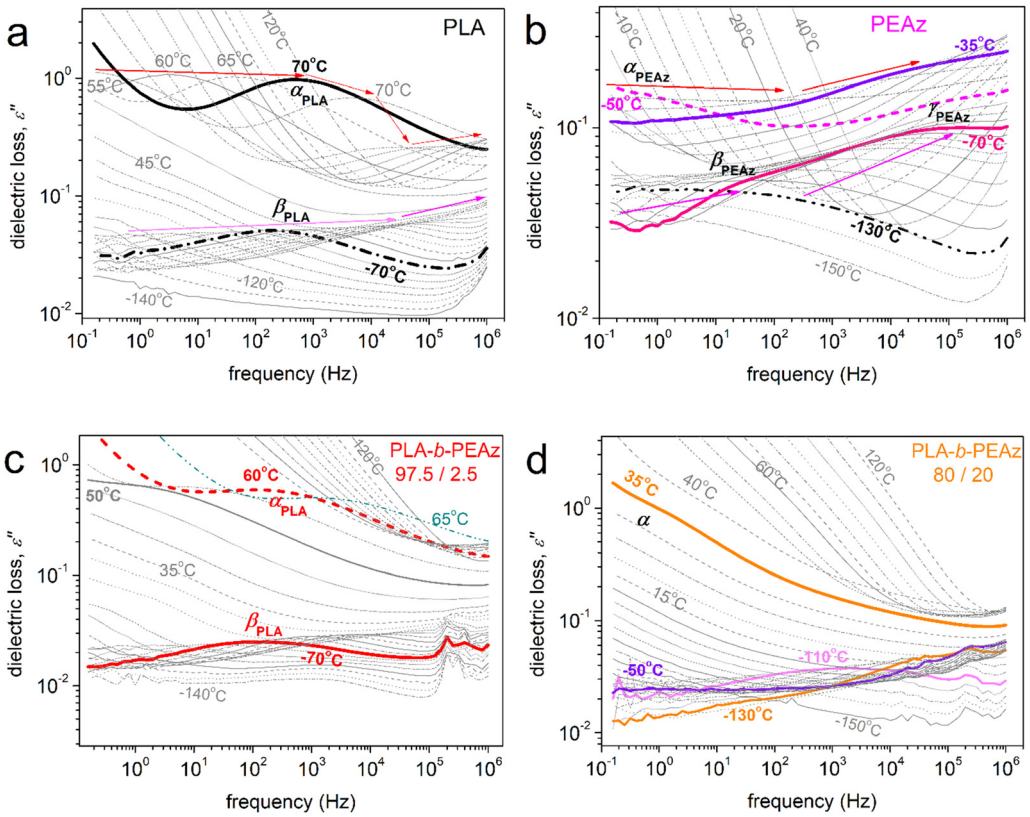

Fig. 10 Raw BDS results in the form of the frequency dependence of the imaginary part of the dielectric permittivity, ε'', as isothermally recorded at various temperatures for the selected samples (descriptions within each figure, a–d). The local and segmental dipolar processes (peaks) are indicated for selected isothermal curves.

peak. This is true for both the low and the higher temperatures, *i.e.*, for local and segmental dynamics. Thus, to extract as much information as possible and conclude with an overall dynamic map, we analysed[80] the complex spectra in terms of known mathematical models, namely the asymmetric Havriliak–Negami (HN)[81] and the symmetric Cole–Cole[56] functions (details in Section S1.5 in the ESI†). In Fig. 12, we present examples of this analysis. Please note that a 'critical' analysis route was followed, *i.e.*, performing many reiterations of the fittings upon evaluating and comparing many parameters and their temperature trends, so that they all make logical sense together. In our case, we uniquely fitted the imaginary permittivity spectra, whereas there have been proposed additional routes, for example, involving the parallel fitting of both ε' and ε''.[82,83]

The results from the analysis/fitting process are summarized in the molecular dynamics maps shown in Fig. 13 and 14. The maps present the reciprocal temperature dependences of the

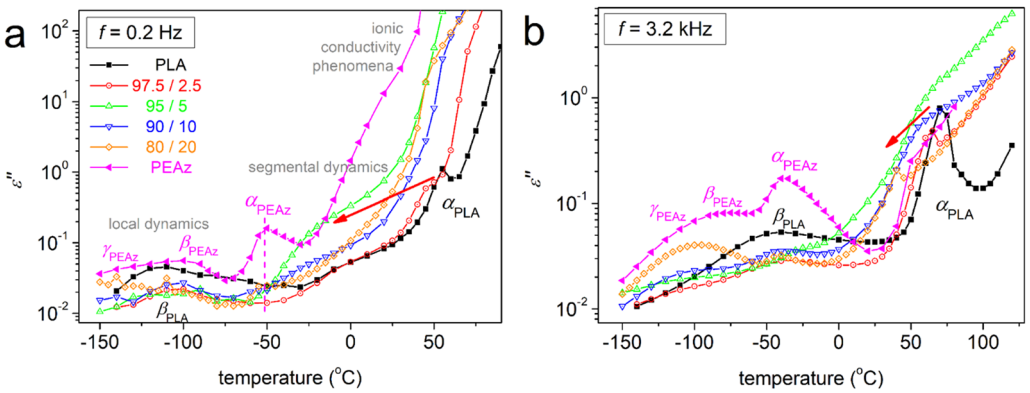

Fig. 11 BDS results shown in terms of isochronal plots of $\varepsilon''(T)$ at the selected frequencies of (a) 0.2 Hz and (b) 3.2 kHz. The resolved local and segmental relaxations (peaks) are indicated within the curves. The added red arrows mark the evolution of segmental relaxation of PLA with increasing PEAz fraction in the copolymers.

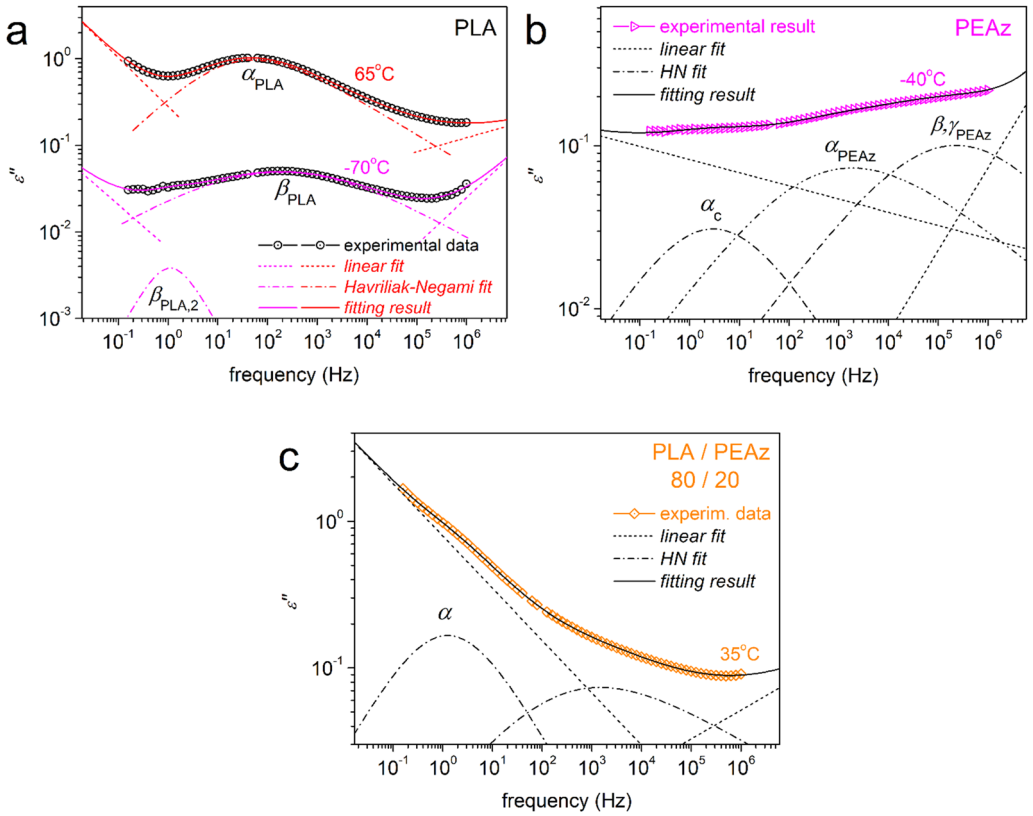

Fig. 12 Analysis of the complex $\varepsilon''(f)$ spectra in terms of model functions, *e.g.*, Havriliak–Negami (HN), shown at the examples of three samples and temperatures, namely, (a) neat PLA at −65 and 70 °C, (b) initial PEAz at −40 °C and (c) copolymer 80/20 at 35 °C.

frequency maxima, $\log f_{max}$, for all the dipolar relaxations (time scale). In these maps, we have added the T_g points as estimated by DSC and TMDSC at appropriate places.

It is essential to first discuss the dynamics in the homopolymers. The situation in PLA is quite well-known and is compatible with previous findings. Except for the strong β_{PLA} (ester group rotation) with an activation energy of $E_{act} \sim 0.45$ eV, the analysis revealed an additional local-like process, *i.e.*, the weaker $\beta_{PLA,2}$ with $E_{act} \sim 0.5$ eV. Another much slower process (1) was also identified; this is extremely weak but necessary for sufficient fitting of the data. Although $\beta_{PLA,2}$ is not trivial in PLA, similar relaxations have been reported.[84,85] It has been proposed that these relaxations may be related to the ester's local mobility being influenced by the early stages of crystallization. For PLA and other polyesters, we have commented on their connection to large-scale mobility (glass transition) and crystallization (Chapter 4 in ref. 86, pp. 87–121).

Coming to neat PEAz in Fig. 13, two local-like relaxations are recorded, namely the fastest and strongest one γ_{PEAz} with $E_{act} \sim 0.44$ eV and the slower and significantly weaker β_{PEAz} with $E_{act} \sim 0.8$ eV. Regarding the origins of these relaxations, we note that PEAz mainly occupies one highly polar site, the –C═O. The fitting shape parameters of both processes (not shown) are quite similar. The differences in time scale and activation suggest that, if arising from the same molecular segment, γ_{PEAz} should express the 'free' (unconstrained) mobility, whereas, β_{PEAz} should display a more constrained mobility. Recalling the fact that PEAz is strongly crystallizable and, making an analogy to semicrystalline PLA,[84] we propose that γ_{PEAz} is activated in the amorphous polymer regions whereas

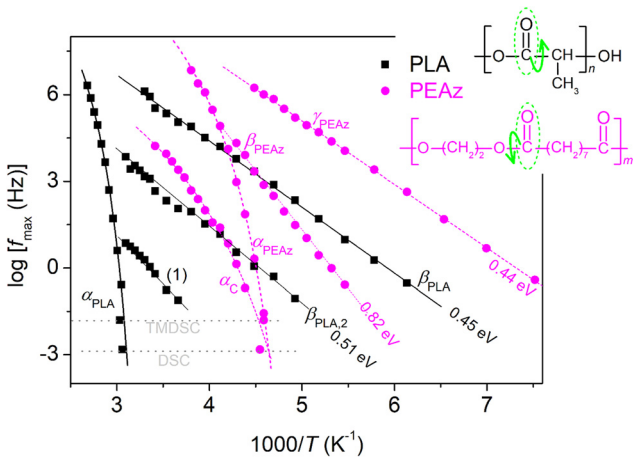

Fig. 13 Dielectric/calorimetric relaxation map for initial PLA and PEAz in terms of the reciprocal temperature (1000/*T*) dependence of the relaxations' frequency maxima, f_{max} (time scale). The corresponding T_g and $T_{g,rev}$ points have been added at the respective equivalent frequencies. The added curved and straight lines connecting the experimental points are fittings of the VFTH and Arrhenius equations, respectively. In the added schematics of the molecular structures of PLA and PEAz, the local motions (crankshaft) related to the β relaxations are described.

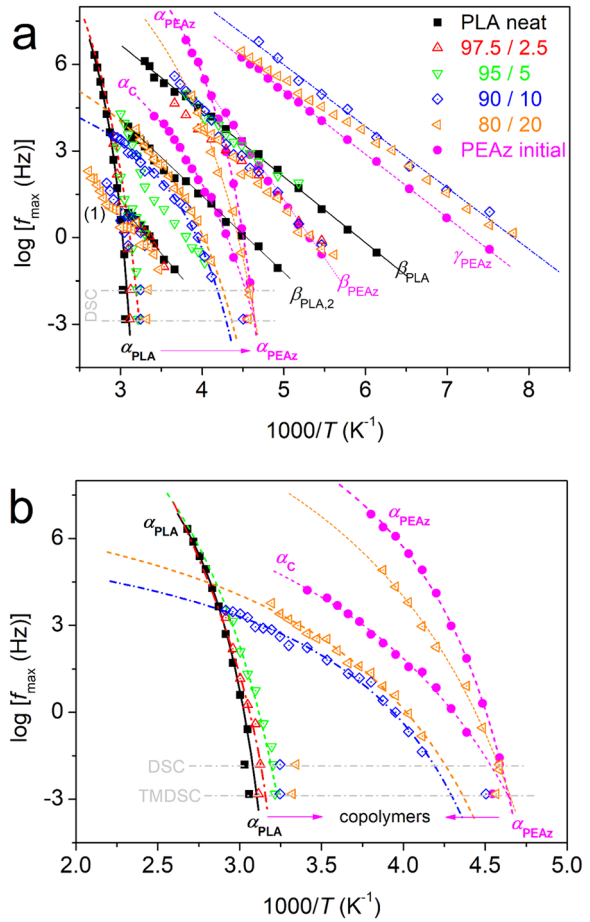

Fig. 14 Dielectric/calorimetric relaxation map for all copolyester compositions and initial PLA and PEAz in terms of time scale, shown for the overall dynamics in (a) and in (b) uniquely for segmental dynamics. The corresponding T_g and $T_{g,rev}$ points have been added at the respective equivalent frequencies. The added lines passing through the experimental points are fittings of the VFTH equation.

β_{PEAz} possibly arises from polymer regions constrained within and/or close to the crystals. Obviously, more work is needed to clarify this point. The segmental dynamics of PEAz are expressed *via* two processes, α-relaxation and another one named 'α_c' here. Both processes exhibit a Vogel–Fulcher–Tammann–Hesse (VFTH) time scale (eqn (S5) in the ESI†),[87] denoting a clear cooperative character. This can be represented from the fragility index, m_α (eqn (S6) in the ESI†), estimated as 118 for α and 65 for α_c. The extrapolation of both time-scales to the corresponding relaxation times of DSC/TMDSC coincides with the calorimetric T_gs (Fig. 13). Finally, the temperature dependence of the dielectric strength, $\Delta\varepsilon$ (Fig. S1 in the ESI†), for α and α_c are opposite, *i.e.*, respectively, decreasing and increasing with T. Considering all these results and comparing with findings from the literature, we propose that α expresses the amorphous unconstrained segmental mobility, whereas α_c arises from segmental mobility of amorphous polymer chains that are constrained by the presence of crystals.[66,84,88–90]

We will now proceed with discussing the effects of the presence of PEAz in the copolymers. Fig. 14 is employed for the said discussion, with the overall dynamics presented in Fig. 14(a) and a focus on the segmental relaxations in Fig. 14(b). The discussion will start from the faster (lower temperatures/higher frequencies) to the slower (higher temperatures) processes.

In the copolymers, the local γ_{PEAz} relaxation could be resolved in only the PEAz-rich systems, *i.e.*, in 90/10 and 80/20 w/w, exhibiting a similar E_{act} and slightly accelerated mobility as compared to neat PEAz. β_{PLA} and β_{PEAz} demonstrate neighbouring time-scales in addition to a crossover at around -50 °C ($1000/T \sim 4.5$ K^{-1}, in Fig. 14(a)). With the exception of 95/5 w/w, within which the β-process is much like that of neat PLA, the β-process in the copolymers tends to be altered in the sense of demonstrating time-scales and E_{act} intermediate to those of β_{PLA} and β_{PEAz}. First, this suggests a continuity and homogeneity in the local dynamics, and it offers indirect evidence that both relaxations arise from similar molecular groups (esteric). The $\beta_{PLA,2}$ process could not be resolved in the copolymers. This could be either due to its absence or due to its very low dielectric strength as compared to the strong segmental dynamics coexisting in the copolymers in these temperature/frequency regions.

Coming to the segmental α-type processes, in Fig. 14(b), one of the most significant findings is that for all compositions, the segmental dynamics are expressed by single relaxations. In Fig. 14(b), it can be easily seen that the presence of PEAz leads to the acceleration of PLA dynamics (horizontal arrows), whereas PEAz dynamics are decelerated by the presence of PLA. This is expected in polymeric blends with quite miscible polymers.[91,92] Herein, the relaxations change in a systematic way when the PLA/PEAz molecular ratio changes. This is important as it denotes, again, the homogeneity in the relaxation times and/or the structure of the relaxing units, in our case the PEAz-*b*-PLA entities. Practically, this is further evidence for the successful copolymer development, noting that such evidence is needed when synthesizing such systems.

In terms of the T_g and fragility index, m, in Fig. 15(a) and (b), respectively, we present the PEAz fraction dependence of both values. The dielectric T_g (PEAz) dependence is monotonic, while for PEAz content higher than 5%, the T_g drop is sharp, suggesting that up to 5% the dynamics of PLA dominate, whereas for higher PEAz fractions, the key role is played by PEAz. This is actually displayed in the dynamics map (Fig. 14(b)) and the $\Delta\varepsilon$ ($1000/T$) (Fig. S2 in the ESI†), wherein the α relaxations seem to be separated into two groups, namely, a PLA-like and PEAz-like behaviour. Please also note that the calorimetric T_g points in Fig. 15(a) demonstrate a similar 'grouping'.

The strong impact of both polymers to each other is also reflected in the variations of m (Fig. 15(b)). The fragility of α_{PLA} is reduced in the copolymers from 139 to ~104–109 for 97.5/2.5 and 95/5 w/w, and down to 75 for 80/20 w/w. The corresponding value for 90/10 w/w cannot be firmly estimated due to the inadequate f_0 value employed in the Boehmer's equation for the fragility[87] (being quite lower than 10^{13} Hz, the necessary value used for performing a consistent m calculation). Besides that, m in the copolymers is lower compared to both initial polymers.

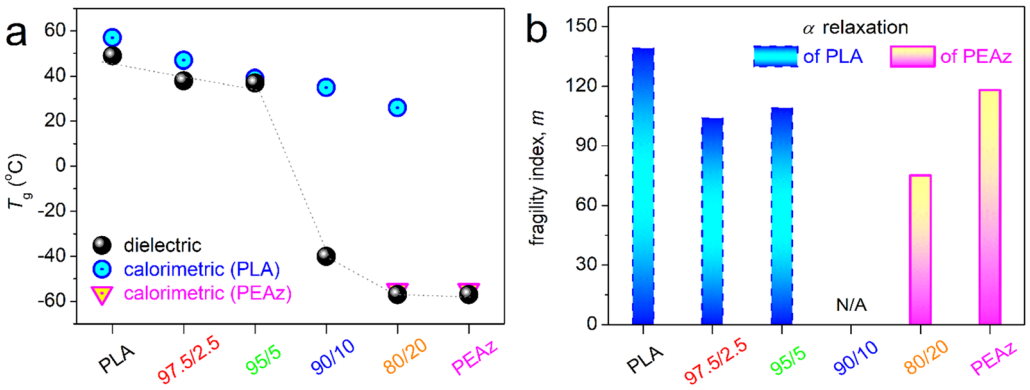

Fig. 15 (a) Dielectric and calorimetric glass transition and (b) fragility index of α relaxation for PLA and PEAz within all samples studied here. The added dotted line in (a) is used to guide the eye in terms of the increasing PEAz content in the samples.

This denotes that the cooperativity level is reduced in the copolymers. To rationalize the effect, we can employ two scenarios, which are however compatible with each other. Always comparing to neat PLA and PEAz, in the first scenario, we expect that in a fixed volume of the copolymer, a smaller number of copolymer chains cooperate with each other, whereas the other scenario suggests that the polymer chains' cooperativity lengths are longer, or else, the inter-chain distances are increased.[93–95] We can visualize that in both scenarios the density of the copolymers is on average decreased, in other words, the free volume is increased. This is in absolute agreement with the previously proposed case of the plasticization effect of PEAz on PLA in the copolymers.[96,97]

We recall that this plasticization effect was a key aim behind preparing PEAz-*b*-PLA and, and our combined findings indicate that this goal has been achieved.

4. Conclusions

The aimed manipulation of the performance of PLA by the presence of PEAz in the form of recently synthesized diblock copolymers is shown in the present article. Next to many results manifesting the successful PEAz-*b*-PLA copolymeric synthesis, which is not an easy task for such systems, we showed that the PEAz block acts as a plasticizer over PLA. This is documented by the systematic drop in T_g and the suppression of the dynamic chain fragility (cooperativity) with increasing PEAz/PLA weight ratio. The strength of this plasticization effect was found to be larger than that imposed by the decrease in the overall molecular weight (M_n). The T_g manipulation was found to be quite large, namely, decades of K. It seems that with PEAz content of up to 5 wt%, PLA is the dominant polymer regarding molecular dynamics and thermal transitions, whereas for 80–90 wt% PLA, PEAz plays the major role. Due to the manifested plasticization, the assumed increase in the free volume and the smaller M_n, the crystallizability of PLA was found to be suppressed in terms of fraction and nucleation. This also led to a variety of semicrystalline morphologies in terms of the size, number, distribution and interconnectivity of the crystals.

Overall, PLA is proved once again to be a polymer that offers for possibilities of manipulations almost at will and *via* relatively mild processing. We expect that the recorded manipulations will have strong impacts on many performance aspects. Recalling that PLA and PEAz-*b*-PLA are actually 'green materials', further study of these systems will be worthwhile. The publication of the article in OA mode was financially supported by HEAL-Link.

Author contributions

Rafail O. Ioannidis: investigation, formal analysis, writing – review & editing. Panagiotis A. Klonos: conceptualization, methodology, investigation, formal analysis, writing – original Draft. Zoi Terzopoulou: investigation, validation, writing – review & editing. Nikolaos Nikolaidis: supervision, investigation, writing – review & editing. Apostolos Kyritsis: resources, validation, writing – review & editing. Dimitrios N. Bikiaris: supervision, resources, validation, writing – review & editing.

Conflicts of interest

There are no conflicts to declare.

Data availability

The DSC, FTIR, XRD and BDS raw data are available on Zenodo (**https://doi.org/10.5281/zenodo.15846386**). The rest of the data supporting this article (estimated values from DSC and dielectric stength values from BDS) have been included as part of the ESI† file. The rest of the data supporting this article will be available upon request to the corresponding authors, uniquely in the frame of private communication.

Acknowledgements

Funded by the European Union under GA no 101070556 (Sustain-a-Print, **https://www.sustainaprint.eu/**). The views and opinions expressed are however those of the authors only and do not necessarily reflect those of the European Union or RIA.

Neither the European Union nor the granting authority can be held responsible for them.

References

1 S. J. Rowan, *ACS Macro Lett.*, 2021, **10**, 466–468.
2 V. Percec and Q. Xiao, *Chem*, 2020, **6**, 2855–2861.
3 J. M. Jafferson and D. Chatterjee, *Mater. Today: Proc.*, 2021, **46**, 1349–1365.
4 R. Mori, *RSC Sustainability*, 2023, **1**, 179–212.
5 R. Blanchard and T. H. Mekonnen, *RSC Appl. Polym.*, 2024, **2**, 557–582.
6 N. M. Ainali, D. Kalaronis, E. Evgenidou, G. Z. Kyzas, D. C. Bobori, M. Kaloyianni, X. Yang, D. N. Bikiaris and D. A. Lambropoulou, *Sci. Total Environ.*, 2022, **832**, 155014.
7 G. Scott, *Polym. Degrad. Stab.*, 2000, **68**, 1–7.
8 G. Chyr and J. M. DeSimone, *Green Chem.*, 2023, **25**, 453–466.
9 J. Sternberg, O. Sequerth and S. Pilla, *Prog. Polym. Sci.*, 2021, **113**, 101344.
10 J. Meegan, *RSC Sustainability*, 2023, **1**, 1737–1742.
11 Z. Terzopoulou and D. N. Bikiaris, *Mater. Lett.*, 2024, **362**, 136174.
12 R. A. Sheldon and M. Norton, *Green Chem.*, 2020, **22**, 6310–6322.
13 M. Hong and E. Y. X. Chen, *Green Chem.*, 2017, **19**, 3692–3706.
14 A. Z. Naser, I. Deiab and B. M. Darras, *RSC Adv.*, 2021, **11**, 17151–17196.
15 R. Auras, B. Harte and S. Selke, *Macrom. Biosci.*, 2004, **4**, 835–864.
16 E. Balla, V. Daniilidis, G. Karlioti, T. Kalamas, M. Stefanidou, N. D. Bikiaris, A. Vlachopoulos, I. Koumentakou and D. N. Bikiaris, *Polymers*, 2021, **13**, 1822.
17 M. Labet and W. Thielemans, *Chem. Soc. Rev.*, 2009, **38**, 3484–3504.
18 L. Kadri, S. Salhi, A. S. Schuller, L. I. Atanase, C. Delaite and H. Ammar, *Polymer*, 2025, **319**, 127981.
19 T. Zhang, B. A. Howell, A. Dumitrascu, S. J. Martin and P. B. Smith, *Polymer*, 2014, **55**, 5065–5072.
20 A. Gandini and T. M. Lacerda, *Macromol. Eng.*, 2022, DOI: 10.1002/9783527815562.mme0019.
21 Y. Zhu, C. Romain and C. K. Williams, *Nature*, 2016, **540**, 354–362.
22 L. I. Atanase, S. Salhi, O. Cucoveica, M. Ponjavic, J. Nikodinovic-Runic and C. Delaite, *Polymers*, 2022, **14**, 1736.
23 G. Z. Papageorgiou, D. N. Bikiaris, D. S. Achilias, E. Papastergiadis and A. Docoslis, *Thermochim. Acta*, 2011, **515**, 13–23.
24 T. Casalini, F. Rossi, A. Castrovinci and G. Perale, *Front. Bioeng. Biotechnol.*, 2019, **7**, 259.
25 L. Sha, Z. Chen, Z. Chen, A. Zhang and Z. Yang, *Int. J. Polym. Sci.*, 2016, **2016**, 6869154.
26 B. Wang, T. Wen, X. Zhang, A. Tercjak, X. Dong, A. J. Müller, D. Wang and D. Cavallo, *Macromolecules*, 2019, **52**, 6274–6284.
27 J. Ahmed and S. K. Varshney, *Int. J. Food. Prop.*, 2011, **14**, 37–58.
28 A. Constanzo, R. Spotorno, M. V. Candal, M. M. Fernández, A. J. Müller, R. S. Graham, D. Cavallo and C. McIlroy, *Addit. Manuf.*, 2020, **36**, 101415.
29 J. Dominguez-Robles, N. K. Martin, M. L. Fong, S. A. Stewart, N. J. Irwin, M. I. Rial-Hermida, R. F. Donnely and E. Larrenta, *Pharmaceutics*, 2019, **11**, 165.
30 P. A. Klonos, K. Chronaki, S. Vouyiouka and A. Kyritsis, *ACS Appl. Polym. Mater.*, 2024, **6**, 1573–1583.
31 P. Saini, M. Arora and M. N. V. Kumar, *Adv. Drug Delivery Rev.*, 2016, **107**, 47–59.
32 D. Garlotta, *J. Polym. Environ.*, 2001, **9**, 63–84.
33 O. Coulembier, J. De Winter, T. Josse, L. Mespouille, P. Gerbaux and P. Dubois, *Polym. Chem.*, 2014, **5**, 2103–2108.
34 S. Saeidlou, M. A. Huneault, H. Li and C. B. Park, *Prog. Polym. Sci.*, 2012, **37**, 1657–1677.
35 M. Rahmanifard, S. M. H. Khademi, R. Asheghi-Oskooee, T. Farizeh and F. Hemmati, *RSC Adv.*, 2024, **14**, 794–807.
36 I. Armentano, N. Bitinis, E. Fortunati, S. Mattioli, N. Rescignano, R. Verdejo, M. A. Lopez-Manchado and J. M. Kenny, *Prog. Polym. Sci.*, 2013, **38**, 1720–1747.
37 R. Zhang, F. Du, K. Jariyavidyanont, E. Zhuravlev, C. Schick and R. Androsch, *Thermochim. Acta*, 2022, **718**, 179387.
38 T. Beslikas, I. Gigis, V. Goulios, J. Christoforides, G. Z. Papageorgiou and D. N. Bikiaris, *Int. J. Mol. Sci.*, 2011, **12**, 6597–6618.
39 T. Zhou, Y. T. Guo, C. Yang, X. B. Meng, F. S. Du and Z. C. Li, *Polym. Chem.*, 2024, **15**, 156–165.
40 A. Toda, R. Androsch and C. Schick, *Polymer*, 2016, **91**, 239–263.
41 R. Androsch, R. Zhang and C. Schick, *Polymer*, 2019, **176**, 227–235.
42 P. A. Klonos, N. D. Bikiaris, P. Barmpalexis and A. Kyritsis, *Polymer*, 2024, **305**, 127177.
43 P. A. Klonos, V. Peoglos, D. N. Bikiaris and A. Kyritsis, *J. Phys. Chem. C*, 2020, **123**, 5469–5479.
44 P. A. Klonos, R. D. Bikiaris, Z. Terzopoulou, K. Mouchlianiti, K. Tsachouridis, A. D. Anastasiou, A. Kyritsis and G. Z. Kyzas, *Polymer*, 2024, **296**, 126841.
45 P. A. Klonos, S. N. Tegopoulos, C. S. Koutsiara, E. Kontou, P. Pissis and A. Kyritsis, *Soft Matter*, 2019, **18**, 1813–1824.
46 Y. Wang, R. J. van Putten, A. Tietema, J. R. Parsons and G. J. M. Gruter, *Green Chem.*, 2024, **26**, 3698–3716.
47 G. Rizis, T. G. van de Ven and A. Eisenberg, *Soft Matter*, 2014, **10**, 2825–2835.
48 J. K. Palacios, J. Zhao, N. Hadjichristidis and A. J. Müller, *Macromolecules*, 2017, **50**, 9683–9695.
49 V. Karava, A. Siamidi, M. Vlachou, E. Christodoulou, A. Zamboulis, D. N. Bikiaris, A. Kyritsis and P. A. Klonos, *Soft Matter*, 2021, **17**, 2439–2453.
50 P. A. Klonos, Z. Terzopoulou, A. Zamboulis, M. A. Valera, A. Mangas, A. Kyritsis, P. Pissis and D. N. Bikiaris, *Soft Matter*, 2022, **18**, 3725–3737.
51 O. Cucoveica, C. Stadoleanu, C. Berstch, R. Triaud, P. Condriuc, L. I. Atanase and C. Delaite, *Polymers*, 2024, **16**, 2748.

52 J. Li, S. Guo, M. Wang, L. Ye and F. Yao, *RSC Adv.*, 2015, **5**, 19484–19492.
53 M. Lazaridou, P. A. Klonos, E. D. Barmpa, A. Kyritsis and D. N. Bikiaris, *Polymer*, 2023, **277**, 125970.
54 R. O. Ioannidis, Z. Terzopoulou, A. Zamboulis, N. D. Bikiaris, M. J. Noordam and N. Nikolaidis, *Mater. Adv.*, 2025, **6**, 2975–2989.
55 R. O. Ioannidis, N. D. Bikiaris, E. Vouvoudi, A. Zamboulis, N. Nikolaidis and D. N. Bikiaris, *Polymers*, 2025, **17**, 1374.
56 F. Kremer and F. Schönhals, *Broadband dielectric spectroscopy*, Springer-Verlag, Berlin, 2002.
57 J. Jeong, M. Ayyood, J. H. Kim, S. W. Nam and Y. J. Kim, *RSC Adv.*, 2019, **9**, 21748–21759.
58 N. D. Bikiaris, P. A. Klonos, R. O. Ioannidis, P. Saranti, P. Barmpalexis and A. Kyritsis, *Polymer*, 2024, **292**, 126635.
59 M. Füllbrandt, P. J. Purohit and A. Schönhals, *Macromolecules*, 2013, **46**, 4626–4632.
60 P. A. Klonos, L. Papadopoulos, G. Z. Papageorgiou, A. Kyritsis, P. Pissis and D. N. Bikiaris, *J. Phys. Chem. C*, 2020, **124**, 10220–10234.
61 P. A. Klonos, N. D. Bikiaris, E. Christodoulou, A. Zamboulis, G. Z. Papageorgiou and A. Kyritsis, *Polymer*, 2022, **242**, 124603.
62 G. Z. Papageorgiou, D. N. Bikiaris, D. S. Achilias and N. Karagiannidis, *Macromol. Chem. Phys.*, 2010, **211**, 2585–2595.
63 P. A. Klonos, N. D. Bikiaris, A. Zamboulis, M. A. Valera, A. Mangas, A. Kyritsis and Z. Terzopoulou, *Soft Matter*, 2023, **19**, 7846–7858.
64 N. D. Bikiaris, A. Kyritsis and P. Barmpalexis, *Mat. Tod. Commun.*, 2024, **38**, 107799.
65 M. Pyda and B. Wunderlich, *Macromolecules*, 2005, **38**, 10472–10479.
66 P. A. Klonos, *Polymer*, 2018, **159**, 169–180.
67 R. Androsch, E. Zhuravlev and C. Schick, *Polymer*, 2014, **55**, 4932–4941.
68 M. C. Righetti, M. Gazzano, M. L. Di Lorenzo and R. Androsch, *Eur. Polym. J.*, 2015, **70**, 215–220.
69 M. C. Righetti, M. Gazzano, N. Delpouve and A. Saiter, *Polymer*, 2017, **125**, 241–253.
70 F. Arai, K. Shinohara, N. Nagasawa, H. Takeshita, K. Takenaka, M. Miya and T. Shiomi, *Polym. J.*, 2013, **45**, 921–928.
71 J. Ren, O. Urakawa and K. Adachi, *Polymer*, 2003, **44**, 847–855.
72 E. Laredo, D. Newman, R. Pezzoli, A. J. Müller and A. Bello, *J. Polym. Sci., Part B: Polym. Phys.*, 2016, **54**, 680–691.
73 A. R. Brás, M. T. Viciosa, Y. Wang, M. Dionísio and J. F. Mano, *Macromolecules*, 2006, **39**, 6513–6520.
74 M. Pluta, J. K. Jeszka and G. Boiteux, *Eur. Polym. J.*, 2007, **43**, 2819–2835.
75 D. E. Martínez-Tong, B. Vanroy, W. Wübbenhorst, A. Nogales and S. Napolitano, *Macromolecules*, 2014, **47**, 2354–2360.
76 J. Leng, P. J. Purohit, N. Kang, D. Y. Wang, J. Falkenhagen, F. Emmerling, A. F. Thüneman and A. Schönhals, *Eur. Polym. J.*, 2015, **68**, 338–354.
77 G. Shi, Y. Guan, G. Liu, A. J. Müller and D. Wang, *Macromolecules*, 2019, **52**, 6904–6912.
78 M. Solar and W. Paul, *Soft Matter*, 2017, **13**, 1646–1653.
79 R. Richert, A. Agapov and A. P. Sokolov, *J. Chem. Phys.*, 2011, **134**, 104508.
80 W. H. Hunter Woodward, in *Broadband Dielectric Spectroscopy: A Modern Analytical Technique*, ed. W. H. Hunter Woodward, American Chemical Society, Washington, DC, 2021, pp. 3–59.
81 S. Havriliak and S. Negami, *Polymer*, 1967, **8**, 161–210.
82 G. P. Baeza, C. Dessi, S. Costanzo, D. Zhao, S. Gong, A. Alegria, R. H. Colby, M. Rubinstein, D. Vlassopoulos and S. K. Kumar, *Nat. Commun.*, 2016, **7**, 11368.
83 A. C. Genix, V. Bocharova, B. Carroll, M. Lehmann, T. Saito, S. Krueger, L. He, P. Dieudonné-George, A. P. Sokolov and J. Oberdisse, *ACS Appl. Mater. Interfaces*, 2019, **11**, 17863–17872.
84 A. R. Brás, M. Dionisio and J. F. Mano, *Macromolecules*, 2008, **41**, 6419–6430.
85 K. Pušnik Črešnar, P. A. Klonos, A. Zamboulis, Z. Terzopoulou, E. Xanthopoulou, L. Papadopoulos, A. Kyritsis, K. Kuzmič, L. Fras Zemljič and D. N. Bikiaris, *Thermochim. Acta*, 2021, **703**, 178998.
86 A. Schönhals and P. Szymoniak, *Dynamics of composite materials*, Springer, Cham, Switzerland, 2022.
87 R. Boehmer, K. Ngai, C. A. Angell and D. J. Plazek, *J. Chem. Phys.*, 1993, **99**, 4201–4209.
88 L. Yu and P. Cebe, *J. Polym. Sci., Part B: Polym. Phys.*, 2009, **47**, 2520–2532.
89 R. Lund, A. Alegría, L. Goitandia, J. Colmenero, M. A. Gonzalez and P. Lindner, *Macromolecules*, 2008, **41**, 1364–1376.
90 M. Soccio, A. Nogales, N. Lotti, A. Munari and T. A. Ezquerra, *Polymer*, 2007, **48**, 4742–4750.
91 S. K. Kumar, S. Shenogin and R. H. Colby, *Macromolecules*, 2007, **40**, 5759–5766.
92 T. P. Lodge, E. R. Wood and J. C. Haley, *J. Polym. Sci., Part B: Polym. Phys.*, 2006, **44**, 756–763.
93 G. Adam and J. H. Gibbs, *J. Chem. Phys.*, 1965, **43**, 139–146.
94 N. Delpouve, A. Saiter and E. Dargent, *Eur. Polym. J.*, 2011, **47**, 2414–2423.
95 C. M. Roland, K. J. McGrath and R. Casalini, *Macromolecules*, 2006, **39**, 3581–3587.
96 R. M. Hodge, T. J. Bastow, G. H. Edward, G. P. Simon and A. J. Hill, *Macromolecules*, 1996, **29**, 8137–8143.
97 G. Wypych, in *Handbook of plasticizers*, ed. G. Wypych, ChemTec Publishing, Elsevier, 3rd edn, 2017, pp. 209–332.

